PLANT SCIENCE

H_2O_2 sulfenylates CHE, linking local infection to the establishment of systemic acquired resistance

Lijun Cao[1,2], Sargis Karapetyan[1,2], Heejin Yoo[1,2]†, Tianyuan Chen[1,2], Musoki Mwimba[1,2], Xing Zhang[1,2], Xinnian Dong[1,2]*

In plants, a local infection can lead to systemic acquired resistance (SAR) through increased production of salicylic acid (SA). For many years, the identity of the mobile signal and its direct transduction mechanism for systemic SA synthesis in initiating SAR have been debated. We found that in *Arabidopsis thaliana*, after a local infection, the conserved cysteine residue of the transcription factor CCA1 HIKING EXPEDITION (CHE) undergoes sulfenylation in systemic tissues, which enhances its binding to the promoter of the SA-synthesis gene *ISOCHORISMATE SYNTHASE1* (*ICS1*) and increases SA production. Furthermore, hydrogen peroxide (H_2O_2) produced through NADPH oxidases is the mobile signal that sulfenylates CHE in a concentration-dependent manner. Accumulation of SA and the previously reported signal molecules, such as *N*-hydroxypipecolic acid (NHP), then form a signal amplification loop to establish SAR.

Systemic acquired resistance (SAR) is an inducible immune mechanism in plants (*1*–*3*) that is triggered by a local immune response and provides long-lasting protection against a wide range of pathogens. This signaling phenomenon and its potential application in agriculture for engineering broad-spectrum disease resistance in crops have led to intense investigation and the discovery that de novo salicylic acid (SA) synthesis in systemic tissues is required for SAR (*4*–*6*). Though exogenous application of SA and its synthetic analogs has been shown to induce SAR without the presence of pathogens (*7*–*9*), how the local defense induces systemic synthesis of SA for biological induction of SAR has remained a mystery. Multiple compounds, such as methyl salicylate, azelaic acid (AzA), dehydroabietinal (DA), glycerol-3-phosphate (G3P), *N*-hydroxypipecolic acid (NHP), and extracellular nicotinamide adenine dinucleotide (phosphate) eNAD(P) (*10*–*16*), have been identified as SAR-inducing signals, with NHP most extensively studied and shown to function synergistically with SA (*3*, *10*, *15*–*23*), but none of them directly activates systemic SA synthesis.

Results

CHE is required for systemic resistance

To identify the missing link between local pathogen infection and systemic SA production, we performed time-course measurements of several known SAR-inducing signals. Previous reports showed that the virulent *Pseudomonas syringae* pv. *maculicola* (*Psm*) ES4326 strain induced a significant NHP increase in uninoculated distal leaves 24 hours postinoculation (hpi), preceding SA induction at 48 hpi (*15*, *20*, *21*, *24*), whereas when the avirulent *Psm* ES4326 strain expressing the effector AvrRpt2 was used, a slight SA induction was detected at 24 hpi (*25*). To reconcile these results, we measured SA, NHP, and G3P in the same samples after mock or *Psm* ES4326/avrRpt2 treatment.

Similar to A. Frank Ross's pioneering SAR experiment in tobacco (*1*), we infected half-leaves of *Arabidopsis thaliana* with *Psm* ES4326/avrRpt2 and collected the infected half-leaves as local and the uninfected half-leaves as neighboring systemic tissues ($systemic_{nbr}$). We also infected two lower leaves with *Psm* ES4326/avrRpt2 and collected the upper uninfected leaves as distal systemic tissues ($systemic_{dist}$). In $systemic_{nbr}$ tissues, we observed increased expression of the SA-synthesis gene *ISOCHORISMATE SYNTHASE1* (*ICS1*) at 8 hpi, preceding the increases in the SA level, the NHP-synthesis gene *FLAVIN-DEPENDENT MONOOXYGENASES* 1 (*FMO1*) expression, and the NHP level at 12 hpi (Fig. 1, A to D). In $systemic_{dist}$ tissues, a significant increase in SA was detected at 16 hpi, whereas increases in NHP and G3P were observed at 24 and 36 hpi, respectively (Fig. 1, E to G). Consistent with *ICS1* expression and SA production being regulated by the circadian clock (*25*), SA levels oscillated, with a trough at 28 hpi. Detection of a robust SA level increase earlier than NHP and G3P in distal tissues after the local *Psm* ES4326/avrRpt2 inoculation suggests that NHP and G3P are unlikely to be signals that are directly responsible for the initial systemic SA synthesis during SAR.

In searching for the direct regulator of systemic SA synthesis, we focused on the circadian clock transcription factor CCA1 HIKING EXPEDITION (CHE), which is required for both basal circadian and pathogen-induced systemic SA production (*25*). To understand CHE's regulatory role in SAR over time, we performed time-course RASL-seq (RNA-mediated oligonucleotide annealing, selection, and ligation with next-generation sequencing) (*26*) to examine expression patterns of approximately 700 selected genes that are primarily involved in defense and SA production. In local tissues, the *che* mutant showed similar overall gene expression patterns and levels of SA, NHP and its precursor pipecolic acid (Pip), and G3P to those of wild type (WT) (Fig. 1H and fig. S1, A and B). This is consistent with the previous finding that the *che* mutant maintains normal local defense (*25*). However, in $systemic_{nbr}$ tissues, *che* displayed fewer transcriptional changes (fig. S1A) and substantially lower production of SA, NHP, and Pip (Fig. 1I and fig. S1C) in response to SAR induction. However, the systemic G3P increase was unaffected in *che* (fig. S1C). These results show that CHE is required for SAR-associated gene expression and accumulation of SA and NHP only in systemic tissues. Interestingly, these CHE-mediated responses did not occur through transcriptional changes in *CALMODULIN BINDING PROTEIN 60g* (*CBP60g*) and *SAR DEFICIENT 1* (*SARD1*), which are involved in SA and NHP synthesis (*17*, *27*); *CIRCADIAN CLOCK-ASSOCIATED 1* (*CCA1*), which is a clock gene targeted by CHE (*28*); or *RESPIRATORY BURST OXIDASE HOMOLOG D* (*RBOHD*), which is known for immune-induced apoplastic reactive oxygen species (ROS) production (*29*–*33*) (fig. S1D).

We next examined effects of *che* on the transportation and sensing of SAR-inducing signal(s) by measuring the activity of petiole exudates (PeX) (*34*–*36*). Notably, PeX from both WT and *che* after *Psm* ES4326/avrRpt2 treatment exhibited a similar capacity to inhibit bacterial growth in WT plants (Fig. 1J), suggesting that *che*, like WT, can produce the SAR-inducing mobile signal(s). However, the inability of *che* to mount a defense in response to PeX treatment indicates that it is defective in sensing the SAR-inducing signal(s). These findings further confirm that CHE is required for SA synthesis and resistance only in systemic tissues.

Cysteine mutants of CHE are defective in SAR

Because neither *CHE* transcript nor protein level showed a substantial increase upon induction in $systemic_{nbr}$ tissues (fig. S2, A and B), we considered protein modifications as an activation mechanism. CHE, also named TCP21, is a class I TCP (TEOSINTE BRANCHED1, CYCLOIDEA, and PCF) transcription factor with a conserved cysteine in the DNA binding domain (*37*). Given that cysteine-containing TCP proteins are sensitive to redox conditions for their DNA-binding activity (*38*) and that the single cysteine residue of CHE (cysteine-51) is conserved across plant species (fig. S2C), we mutated it and found that, unlike the WT CHE tagged with hemagglutinin (HA) under its native promoter (*CHE-HA/che-2*), cysteine mutants che^{CS}*-HA/che-2* (cysteine to serine) and che^{CW}*-HA/che-2* (cysteine to tryptophan)

[1]Department of Biology, Duke University, Durham, NC 27708, USA. [2]Howard Hughes Medical Institute, Duke University, Durham, NC 27708, USA.
*Corresponding author. Email: xdong@duke.edu
†Present address: School of Biological Science, University of Utah, Salt Lake City, UT 84112, USA.

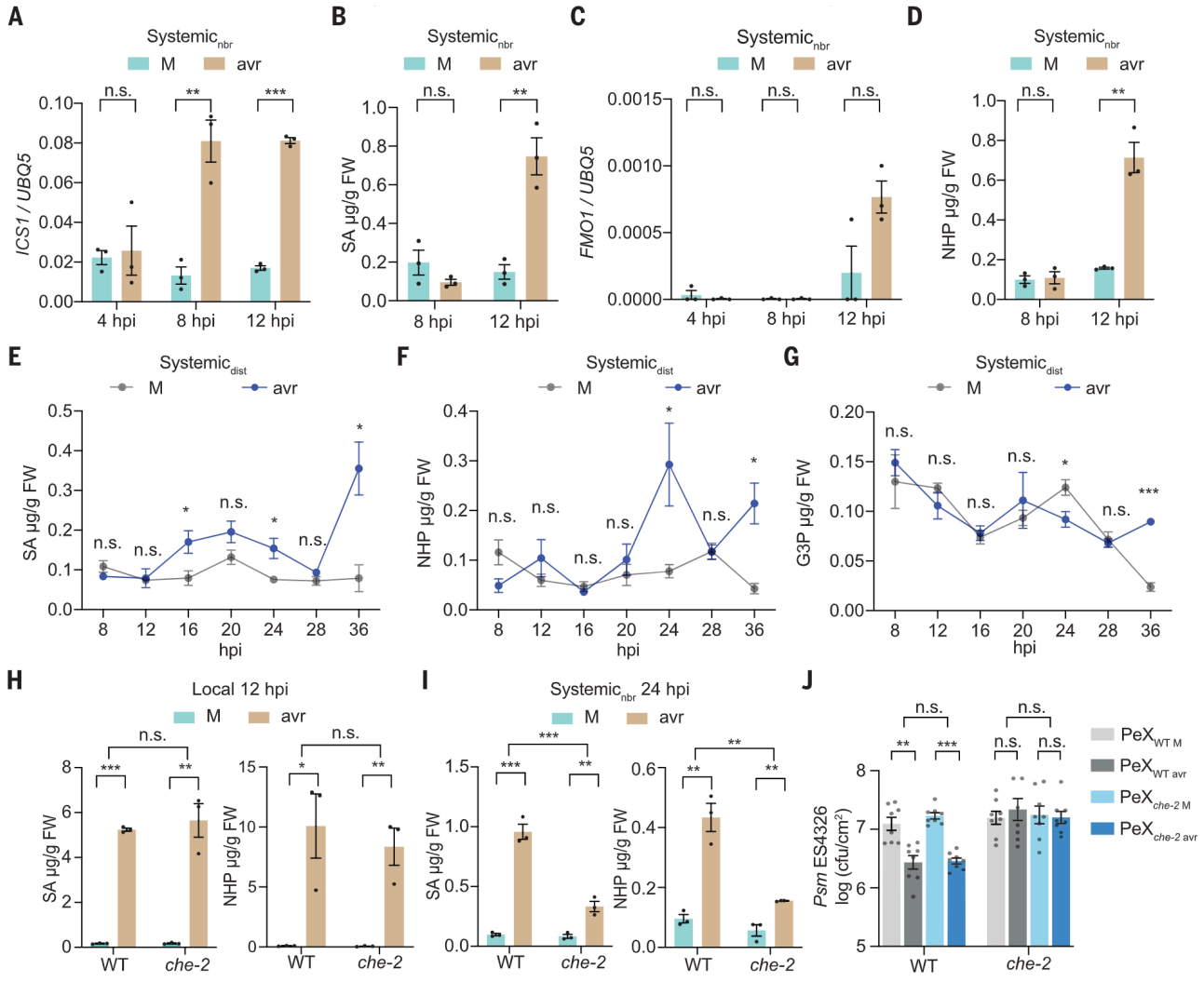

Fig. 1. CHE is required for systemic SA and NHP production. (**A** to **D**) Time-course measurements of *ICS1* expression (A), SA level (B), *FMO1* expression (C), and NHP level (D) in the neighboring untreated half-leaf (systemic$_{nbr}$) tissues after inoculation of the other half with mock (M; 10 mM $MgCl_2$) or *Psm* ES4326/avrRpt2 [avr; optical density at 600 nm (OD_{600}) = 0.01]. Data are mean ± SEM (n = 3). (**E** to **G**) Time-course measurements of SA (E), NHP (F), and G3P (G) in the uninoculated distal leaf (systemic$_{dist}$) tissues after local M or avr treatment. Data are means ± SEM (n = 3). (**H** and **I**) Levels of SA and NHP in the treated half-leaves (local) (H) and systemic$_{nbr}$ tissues (I) in WT and the *che-2* mutant. Data are means ± SEM (n = 3). (**J**) Bacterial growth in WT and *che-2* plants pretreated with PeX collected from WT or *che-2* plants after M or avr treatment. Data are means ± SEM (n = 8). Significant differences were calculated using either two-tailed Student's t tests or two-way analysis of variance (ANOVA). ***P < 0.001, **P < 0.01, *P < 0.05, and n.s. is not significant.

failed to complement *che-2* in inducing systemic *ICS1*, *FMO1*, and *PR1* (fig. S3A). Further analysis of the *che^{CS}-HA* line revealed a similar defect in the expression of other SA synthesis–related genes, namely, *AVRPPHB SUSCEPTIBLE 3* (*PBS3*) and *ENHANCED DISEASE SUSCEPTIBILITY 5* (*EDS5*), but not the nonessential gene *ENHANCED PSEUDOMONAS SUSCEPTIBILITY 1* (*EPS1*) (*39*, *40*) (fig. S3B), and compromised induction of SA and NHP compared with the *CHE-HA* line (Fig. 2, A and B).

To examine the effect of the cysteine mutation on CHE's transcriptional activity, we performed chromatin immunoprecipitation–quantitative PCR (ChIP-qPCR). In systemic$_{nbr}$ tissues, we observed a significant increase in CHE-HA binding to the TCP-binding site (TBS) of the *ICS1* promoter (*ICS1$_P$*) compared with the control (*ICS1$_{PControl}$*) carrying the SARD1-binding site, whereas this increase was compromised in *che^{CS}-HA* transgenic lines (Fig. 2C). The *che^{CS}-HA* mutant was also defective in response to exogenous SA treatment (Fig. 2D), consistent with the previous finding that *che* mutants are defective in SA-mediated SAR signal amplification (*25*). However, the binding of CHE to the TBS of the *EDS5* promoter (*EDS5p*) was not affected by SAR induction (fig. S3C) nor was the promoter of *CCA1* (*CCA1p*) (*28*) (Fig. 2, E and F). Consistently, *che^{CS}-HA* could rescue the short-period phenotype of the *che-1 lhy-20* double mutant (*28*) (fig. S4, A and B). Additionally, we found that promoters of *AGD2-LIKE DEFENSE RESPONSE PROTEIN 1* (*ALD1*) and *FMO1* do not have known TBS or binding activity with CHE (fig. S5, A and B), suggesting that CHE does not directly regulate these genes. Further supporting that the cysteine residue of CHE modulates its binding to the *ICS1* promoter to activate systemic SA synthesis, neither *che^{CS}-HA* nor *che^{CW}-HA* could rescue the SAR deficiency of the *che* mutants (*25*) (Fig. 2, G and H, and fig. S3D).

CHE is sulfenylated in an H_2O_2 concentration–dependent manner

To investigate how CHE initiates SAR, we focused on its cysteine residue. Because CHE has only one cysteine residue, formation of a disulfide bond would require a cysteine-containing partner, which was not detected using nonreducing

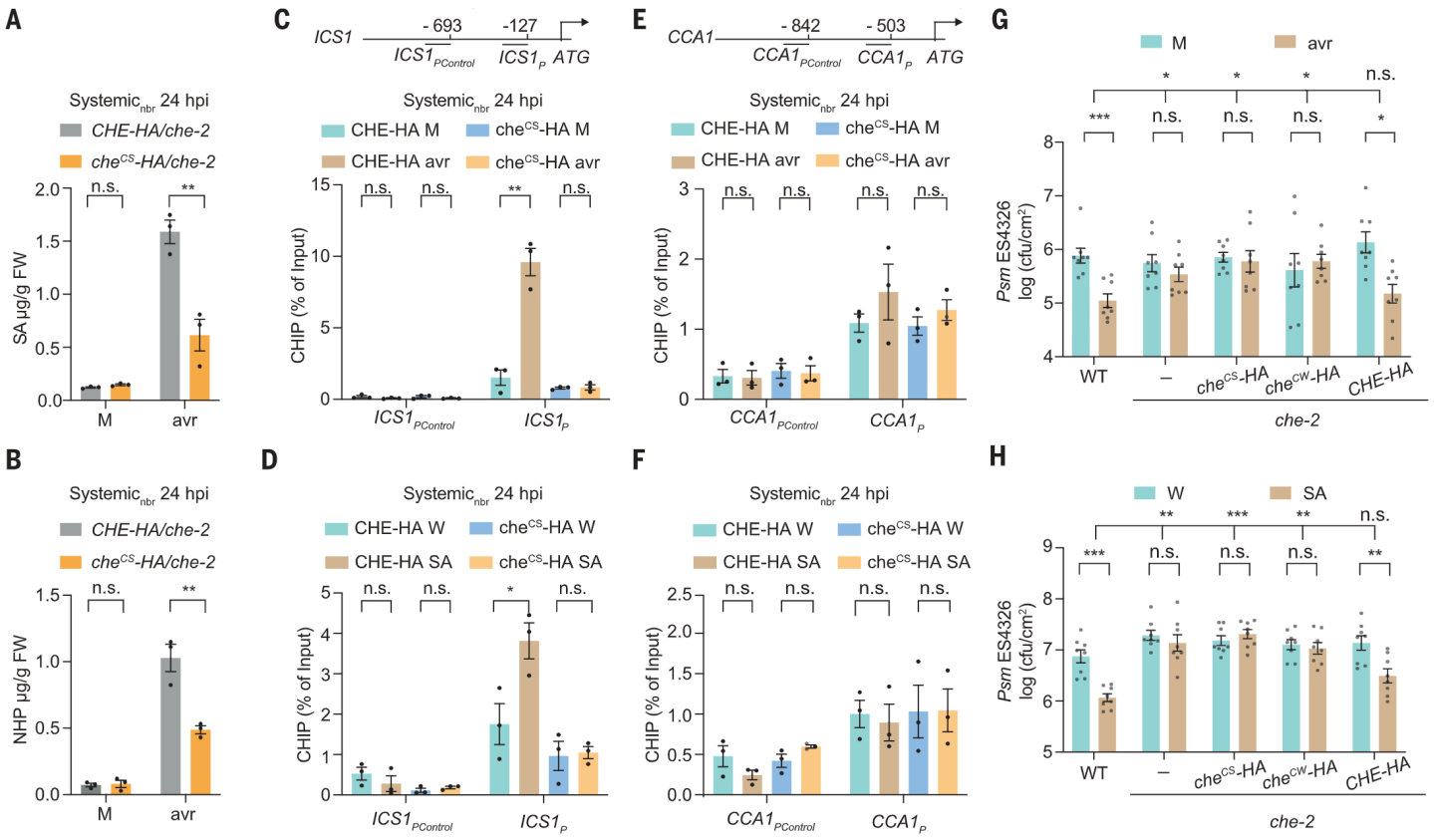

Fig. 2. The cysteine residue in CHE is required for SAR. (**A** and **B**) SA (A) and NHP (B) in untreated half-leaf (systemic$_{nbr}$) tissues after mock (M; 10 mM $MgCl_2$) or *Psm* ES4326/avrRpt2 (avr; OD_{600} = 0.01) treatment. *CHE-HA/che-2* and *che^{CS}-HA/che-2* indicate WT CHE and the cysteine-to-serine mutant in *che-2* background, respectively. Data are means ± SEM (*n* = 3). FW, fresh weight. (**C** and **D**) ChIP-qPCR of CHE-HA and che^{CS}-HA binding to the *ICS1* promoter (*ICS1$_P$*) after avr treatment (C) and after water (W) or SA treatment (D). Data are means ± SEM (*n* = 3). (**E** and **F**) ChIP-qPCR of CHE-HA and che^{CS}-HA binding to the *CCA1* promoter (*CCA1$_P$*). Data are means ± SEM (*n* = 3). (**G**) Bacterial growth. Plants were inoculated with M or avr 2 days before infecting distal leaves with *Psm* ES4326 (OD_{600nm} = 0.001), and bacterial growth was measured 3 days after the second inoculation. *che^{CW}-HA/che-2* indicates the cysteine-to-tryptophan mutant. Data are means ± SEM (*n* = 8). (**H**) Bacterial growth 1 day after SA treatment. Data are means ± SEM (*n* = 8). Significant differences were calculated using either two-tailed Student's *t* tests or two-way ANOVA. ***$P < 0.001$, **$P < 0.01$, *$P < 0.05$, and n.s. is not significant.

SDS gel electrophoresis under mock or induced conditions (fig. S2B). We therefore performed biotin-switch assays (*41*) to capture CHE with other possible modifications by ROS, such as S-sulfenylation (SOH), S-sulfinylation (SO_2H) (*42*), and S-nitrosylation by reactive nitrogen species (*41*, *42*) using modification-specific reducing agents. Notably, we found that CHE is sulfenylated (CHE-SOH) starting from 8 hpi in systemic$_{nbr}$ tissues (Fig. 3A and fig. S6A), consistent with the time of *ICS1* induction (Fig. 1A). In systemic$_{dist}$ tissues, CHE-SOH was also detected, starting at 16 hours after *Psm* ES4326/avrRpt2 inoculation (Fig. 3B), coinciding with an SA increase in distal tissues (Fig. 1E). Inoculation with *Psm* ES4326 led to CHE-SOH at around 24 hpi (Fig. 3B). These findings show that CHE-SOH occurs earlier in neighboring tissues than in distal tissues and faster after a local infection with *Psm* ES4326/avrRpt2 than with *Psm* ES4326. Additionally, exogenous SA application led to CHE-SOH at 24 hours after treatment (fig. S6B). To determine whether CHE can be sulfenylated in vitro, we treated purified CHE with various H_2O_2 concentrations because H_2O_2 is produced during defense responses and induces microscopic cell death in systemic tissue to enhance resistance (*33*, *43*–*45*). Interestingly, we found that CHE is sulfenylated specifically at around 40 to 50 µM H_2O_2, whereas lower or higher concentrations did not result in this modification, as shown by the biotin-switch results (Fig. 3C and fig. S6C).

To determine whether the enhanced binding of CHE to the *ICS1* promoter (Fig. 3, D and E) is due to sulfenylation, we performed a gel electrophoresis mobility shift assay using a DNA probe containing the *ICS1* TBS (*TBSi*). We found that treatment with 50 µM H_2O_2 markedly enhanced CHE binding to *TBSi* in vitro (Fig. 3F). This increase was due to CHE-SOH because treatment with *m*-arsenite, a reducing agent specific for SOH, diminished the binding. Moreover, the H_2O_2-induced binding was largely absent in che^{CS}-HA mutant protein, confirming that sulfenylation of CHE is the molecular switch that increases its binding to the *ICS1* promoter. Additionally, we observed increased sulfenylation of *N. benthamiana* CHE homologs NbTCP21-1 and NbTCP21-2 (*46*) after treatment with *P. syringae* pv. *tomato* DC3000 (*Pst*) (Fig. 3G), an avirulent pathogen for *N. benthamiana* (*47*). These results suggest that CHE sulfenylation is a conserved mechanism for systemic SA synthesis during SAR.

To understand why CHE-SOH is only detected in systemic tissues, we hypothesized that higher ROS levels in local tissues might further oxidize the cysteine residue in CHE. We found that this was indeed the case because whereas sulfenylation (CHE-SOH) was observed in systemic tissues, sulfinylation (CHE-SO_2H) was detected in local tissues (Fig. 3H) using the reacting agent specific for sulfinic acid, DiaAlk (*48*). Regardless of whether CHE-SO_2H can be further oxidized to CHE-SO_3H in local tissues, neither form is active in binding to the *ICS1* promoter (Fig. 3D). This H_2O_2 concentration–specific activation of CHE may also explain the controversy over H_2O_2's role as a defense signal in previous studies, in which different H_2O_2 concentrations were used (*49*, *50*).

H_2O_2 serves as a mobile signal for SAR

Because in vitro H_2O_2 treatment enhanced CHE's binding to the *ICS1* promoter (Fig. 3, C and F), we investigated H_2O_2 as an endogenous signal for activating CHE by measuring H_2O_2 levels in systemic$_{nbr}$ and systemic$_{dist}$ tissues after induction by *Psm* ES4326/avrRpt2 and *Psm* ES4326. As expected, higher H_2O_2 induction was detected in the local tissues (~20 μmol/m^2) than in systemic$_{nbr}$ tissues (~15 μmol/m^2) from 4 hpi (Fig. 4A and fig. S7A). Interestingly, this increase was not significantly affected in *che*, except at 24 hpi (Fig. 4A), or in the *ald1* or *fmo1* mutants, but it was abolished in the *SALICYLIC ACID INDUCTION DEFICIENT 2* (*sid2*) mutant of *ICS1 (51)* and in *rbohD* (fig. S7, B and C). In systemic$_{dist}$ tissues, H_2O_2 production started to increase later, at around 12 hpi for *Psm* ES4326/avrRpt2 and 24 hpi for *Psm* ES4326 (Fig. 4B). H_2O_2 levels in PeX collected from *che* and NHP-deficient *ald1* and *fmo1* mutants increased similarly to WT after infection, whereas no increase was detected in *rbohD* (Fig. 4C), demonstrating that H_2O_2 production in PeX requires RBOHD but not NHP. Moreover, SA and NHP treatments could induce H_2O_2, similarly to pathogen treatment (fig. S8, A and B). However, the NHP-mediated H_2O_2 production and subsequent CHE-SOH were abolished in the *sid2* mutant (fig. S8, B and C), which indicated dependency on SA and was consistent with previous reports of an amplification loop involving SA, NHP, and H_2O_2 (*20*, *21*, *49*, *52*).

To monitor ROS (e.g., H_2O_2) transport from local to systemic tissues during SAR induction, we utilized a live-imaging technique using 2′,7′-dichlorodihydrofluorescein diacetate (*53*, *54*). Upon *Psm* ES4326/avrRpt2 inoculation, ROS signals were detected in both WT and *fmo1* plants in local and, subsequently, in systemic$_{nbr}$ tissues (Fig. 4D and movies S1 and S2), indicating that this ROS signaling is independent of NHP production. To measure this signaling process at the whole-plant level, we used a luciferase reporter driven by the ROS-responsive promoter of *GLUTAREDOXIN 13* (*GRXS13*) (*55*). After *Psm* ES4326/avrRpt2 challenge, ROS accumulated in systemic$_{nbr}$ and systemic$_{dist}$ tissues at approximately 8 and 16 hpi, respectively (movies S3 and S4), which aligned with the time of detection for H_2O_2 and CHE-SOH (Figs. 3, A and B, and 4, A and B), but before the reported detection of other mobile signals such as G3P, Aza, DA, and NHP (*12*–*15*, *20*, *21*, *23*, *56*). When *Psm* ES4326 was used as the inducer, ROS accumulation in the systemic$_{nbr}$ and systemic$_{dist}$ tissues occurred at approximately 12 and 20 hpi, respectively, which was delayed by several hours compared with *Psm* ES4326/avrRpt2 challenge (movies S5 and S6). Consistent with the measurements (Fig. 4C and fig. S7, B and C), ROS production and transport were compromised in the *rbohD* mutant (Fig. 4D and movie S7). RBOHD and its homolog RBOHF catalyze H_2O_2 production by transferring electrons to oxygen to form superoxide anion (O_2^-), which is converted to H_2O_2 (*57*). In support of an essential role of RBOHD and RBOHF in initiating SAR, the *rbohD* mutant is deficient in CHE-SOH, CHE binding to the *ICS1* promoter, *ICS1* induction, and, along with *rbohF*, SAR (Fig. 4E and fig. S9, A to C). These findings demonstrate that NADPH oxidase RBOHD/F-produced H_2O_2 is an initiating mobile signal for establishing SAR.

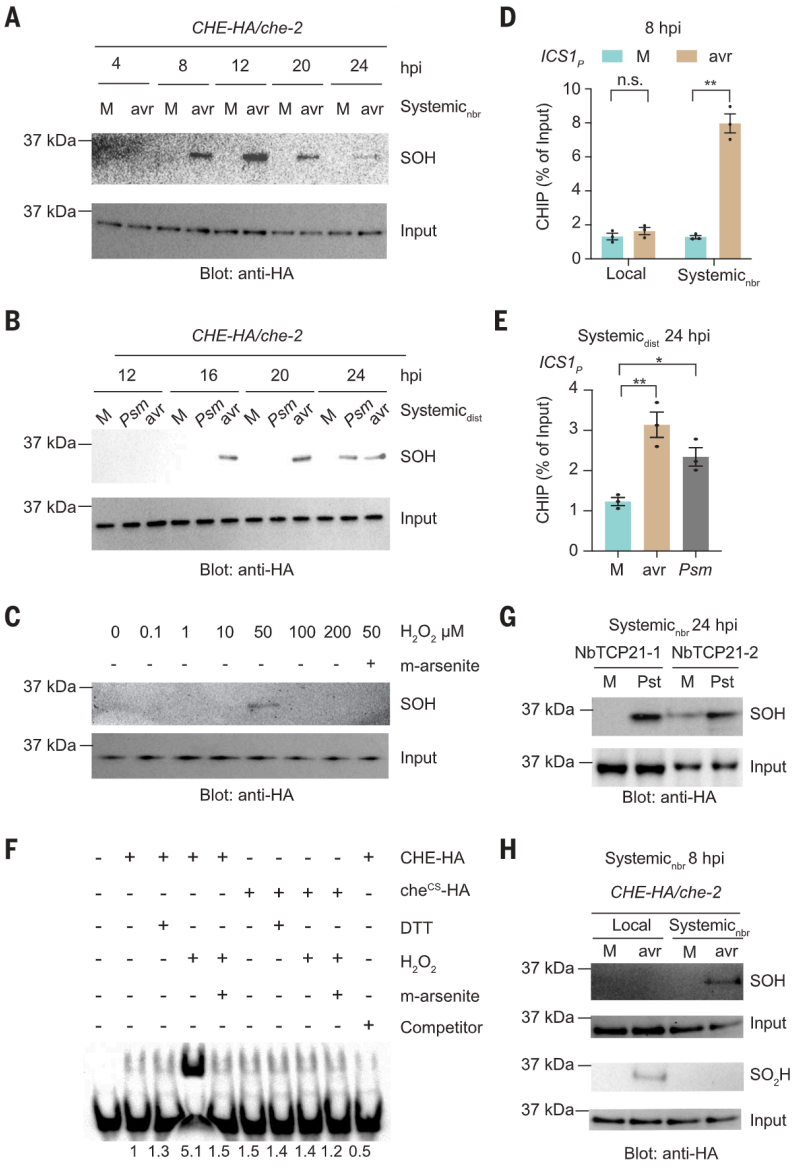

Fig. 3. CHE-SOH occurs specifically in systemic tissues. (**A**) Immunoblots showing sulfenylation (SOH) of CHE in the untreated half-leaf (systemic$_{nbr}$) tissues after mock (M; 10 mM $MgCl_2$) or *Psm* ES4326/avrRpt2 (avr; OD_{600} = 0.01) treatment. *CHE-HA/che-2* indicates transgenic plants expressing WT CHE tagged with HA under its native promoter in *che-2* background. (**B**) Immunoblots showing CHE-SOH in the distal leaf (systemic$_{dist}$) tissues triggered by avr or *Psm* ES4326 (*Psm*; OD_{600} = 0.01). (**C**) Immunoblots showing in vitro CHE-SOH after H_2O_2 treatment. Sodium arsenite (*m*-arsenite) is a reducing agent that specifically removes sulfenylation. (**D** and **E**) ChIP-qPCR of CHE-HA binding to the *ICS1* promoter carrying the TCP-binding site ($ICS1_P$) in the treated half-leaves (local) and systemic$_{nbr}$ (D) or systemic$_{dist}$ (E) tissues. Data are means ± SEM (*n* = 3). (**F**) Electrophoresis mobility shift assay of recombinant CHE protein binding to the TBS-containing DNA probe from the *ICS1* promoter (*TBSi*). (**G**) Immunoblots showing sulfenylation of *N. benthamiana* CHE homologs, NbTCP21-1 and NbTCP21-2 tagged by HA, in systemic$_{nbr}$ tissues after mock or *Pseudomonas syringae* pv. *tomato* DC3000 treatment of *N. benthamiana* plants. (**H**) Immunoblots showing SOH or sulfinylation (SO_2H) of CHE in local and systemic$_{nbr}$ tissues. Significant differences were calculated using two-tailed Student's *t* tests. $^{**}P < 0.01$, $^{*}P < 0.05$, and n.s. is not significant.

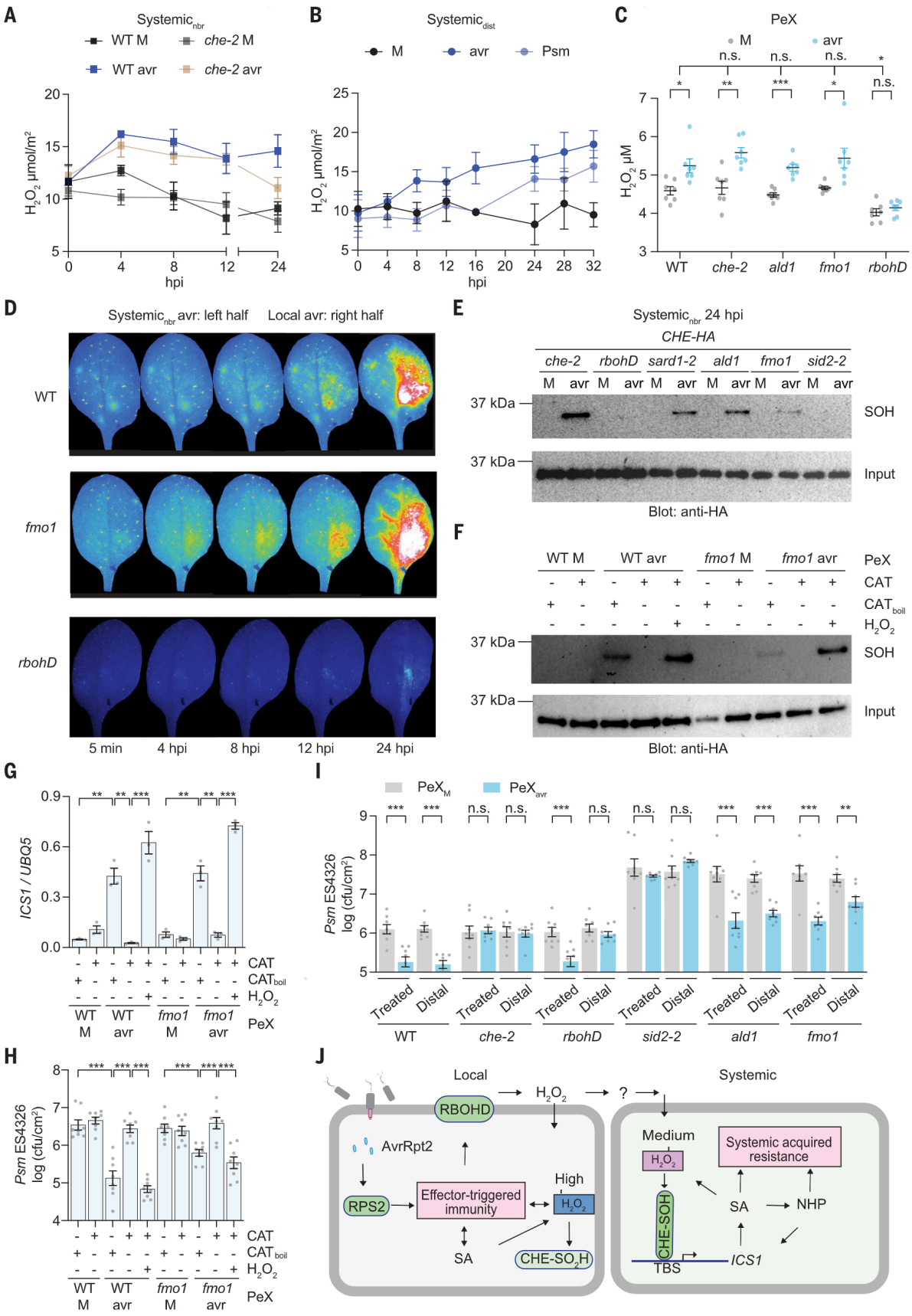

Fig. 4. H_2O_2 initiates SAR. (**A** and **B**) H_2O_2 production in the untreated half-leaf (systemic$_{nbr}$) (A) or distal leaf (systemic$_{dist}$) (B) tissues after mock (M; 10 mM $MgCl_2$), *Psm* ES4326/avrRpt2 (avr; OD_{600} = 0.01), or *Psm* ES4326 (*Psm*; OD_{600} = 0.01) treatment. Data are means ± SEM (n = 5). (**C**) PeX H_2O_2 levels. Data are means ± SEM (n = 7). (**D**) Snapshots of ROS imagings using 2′,7′-dichlorodihydrofluorescein diacetate. (**E**) Immunoblots showing sulfenylation (SOH) of CHE. (**F** to **H**) The effect of PeX on CHE-SOH (F) (immunoblots), *ICS1* expression (G), and bacterial growth (H) in WT plants. Data are means ± SEM [n = 3 for (G);

n = 8 for (H)]. CAT_{boil}, boiled catalase. (**I**) Bacterial growth in the PeX-treated or distal leaves. Data are means ± SEM (*n* = 8). (**J**) The model. Local defense results in high H_2O_2 accumulation and CHE sulfinylation (CHE-SO_2H) without increasing CHE's *ICS1* promoter-binding activity. Local defense activates RBOHD to produce H_2O_2, which accumulates to a moderate level in systemic tissues to sulfenylate CHE; this enhances CHE's binding to the *ICS1* promoter to induce systemic SA synthesis and initiate SAR. Full-scale resistance is achieved through the synergistic activities of SA, NHP, and perhaps other signals. Significant differences were calculated using either two-tailed Student's *t* tests or two-way ANOVA. ***$P < 0.001$, **$P < 0.01$, *$P < 0.05$, and n.s. is not significant.

PeX H_2O_2 initiates SA synthesis in establishing SAR

To demonstrate that H_2O_2 is the signal that sulfenylates CHE and establishes SAR in systemic tissues, we measured SA, NHP, and G3P in PeXs collected from WT and *fmo1*. After *Psm* ES4326/avrRpt2 induction, NHP levels significantly increased in WT PeX but not in *fmo1* (fig. S9D). Additionally, a slight G3P elevation was also detected, whereas SA was undetectable in PeX from both WT and *fmo1*, confirming that SA is synthesized de novo in systemic tissues (*5*). To demonstrate that H_2O_2 is the initial mobile signal for systemic SA synthesis, we treated PeX collected from both WT and *fmo1* with catalase to deplete H_2O_2 (fig. S9E) and found that it abolished PeX's ability to sulfenylate CHE (Fig. 4F); induce expression of *ICS1*, *FMO1*, and *PR1* (Fig. 4G and fig. S9, F and G); and enhance resistance against *Psm* ES4326 in WT plants (Fig. 4H). This inhibitory effect of catalase was eliminated by heat denaturation (CAT_{boil}) and overcome by adding back H_2O_2 after removing catalase. Importantly, PeX from *fmo1*, which lacked NHP (fig. S9D), still elicited significant SAR responses, albeit slightly less than WT (Fig. 4H and fig. S9F), consistent with previous reports that PeX from the NHP-deficient *ald1* mutant could still trigger systemic defense (*58*, *59*). These results further support that H_2O_2 is required for CHE activation through sulfenylation to initiate systemic SA synthesis, whereas NHP contributes to SA accumulation through a mutual amplification loop (*20*, *21*). Consistently, CHE-SOH was detected, with a reduction, in mutants of *ALD1*, *FMO1*, and *SARD1* (Fig. 4E), whose own expression is SA-inducible (*17*, *27*), confirming their role in the amplification loop. Furthermore, NHP-induced SAR was found to be dependent on RBOHF-produced ROS and eNAD(P) (*10*), and treating plants with NAD(P) increased both H_2O_2 production and CHE-SOH (fig. S9, H and I).

Interestingly, although SAR-competent PeX could activate defense in both treated and distal leaves of WT plants, it failed to trigger the response in distal leaves of *rbohD* (Fig. 4I), indicating that RBOHD is required for the relay production of H_2O_2 to induce SAR. Unlike *rbohD*, *che* and *sid2* were nonresponsive to PeX in either treated or distal tissues (Fig. 4I), supporting our conclusion that, in systemic tissues, CHE-mediated *ICS1* induction is required for SAR initiation and establishment. As expected, the *ald1* and *fmo1* mutants retained partial responsiveness to PeX while displaying a defect in basal resistance, in contrast to the *che* and *rbohD* mutants (gray bars in Fig. 4I).

Discussion

Our study reveals that NADPH oxidase–generated H_2O_2 is the primary signal initiating SAR by sulfenylating CHE and inducing de novo SA production in systemic tissues (Fig. 4J). This initial SA increase has likely been overlooked in earlier studies owing to its relative subtlety compared with the large SA increase that occurs because of the amplification loop. By using time-course measurements as well as live imaging (Figs. 1E and 4B, and movies S1 to S6), we were able to capture these early signaling events. It will be interesting to investigate whether and how NHP, G3P, eNAD(P) (*10*), and nitric oxide (*59*–*62*) are involved in the relay production of H_2O_2 in coordination with RBOHD. Our study also lays the groundwork for exploring how systemic H_2O_2, SA, NHP, and other signals form an amplification loop to confer full-scale SAR (Fig. 4I). Though the complete circuitry of this amplification loop has yet to be elucidated (Fig. 4J), one study showed that SA can increase H_2O_2 production by inhibiting catalase activity, resulting in sulfenylation of tryptophan synthetase β SUBUNIT 1 to suppress auxin biosynthesis and confer resistance (*52*).

Although necrotizing pathogens were initially used in the search for ways to "vaccinate" plants and trigger SAR (*1*), virulent pathogens, such as *Psm* ES4326, could also induce SAR (*10*, *63*, *64*), albeit with a delay (Figs. 3B and 4B). We hypothesize that *Psm* ES4326, despite not causing noticeable programmed cell death, contains other effectors that can not only produce damage-associated molecular patterns but also be weakly recognized by immune receptors other than RESISTANT TO P. SYRINGAE 2 (RPS2), because mutating these receptors partially inhibits *Psm* ES4326/avrRpt2-mediated programmed cell death and resistance in the presence of RPS2 (*65*). Different strains of pathogens carry distinct sets of effectors, whose interactions with host targets may trigger other signaling events besides the one identified in this study (*63*, *64*, *66*, *67*). Using effector-triggered immunity–inducing avirulent pathogens could simplify the study because they could more quickly induce sufficient H_2O_2 through effector-triggered immunity in local tissues to trigger SAR.

It is intriguing that a circadian clock transcription factor (i.e., CHE) controls SAR induction in plants, raising questions about the biological importance of this connection. Because mutating the cysteine in CHE does not affect its clock function (Fig. 2, E and F, and fig. S4), CHE's role in SAR is unlikely through the circadian clock. Previously, we showed that effector-triggered immunity–associated programmed cell death is gated by the redox rhythm toward the morning (*68*). Therefore, CHE's peak expression around dusk (fig. S2A) aligns with the time when the H_2O_2 signal, produced in the morning, reaches systemic tissues (Fig. 4B and movies S1 and S4), sulfenylating CHE throughout the night (Fig. 3, A and B) to induce robust SAR in the morning when conditions, such as high humidity, favor many pathogens (*25*, *69*–*71*).

Our finding that an optimal H_2O_2 concentration is required to sulfenylate CHE reconciles conflicting reports on H_2O_2's role in defense (*49*, *50*) because higher-than-optimal H_2O_2 levels would inactivate CHE in inducing *ICS1* by further oxidizing CHE (Fig. 3, D and H). It is tempting to hypothesize that the sensitivity to H_2O_2 concentration allows plants to gauge the level of local infection to determine whether and how much to activate SAR. Therefore, our study not only identifies H_2O_2 as the primary mobile signal and H_2O_2-mediated CHE-SOH as the signal transduction mechanism in inducing systemic SA synthesis but also conforms with previous discoveries on SAR activation after local infection (*1*–*3*, *20*).

REFERENCES AND NOTES

1. A. F. Ross, *Virology* **14**, 340–358 (1961).
2. Z. Q. Fu, X. Dong, *Annu. Rev. Plant Biol.* **64**, 839–863 (2013).
3. A. C. Vlot *et al.*, *New Phytol.* **229**, 1234–1250 (2021).
4. T. Gaffney *et al.*, *Science* **261**, 754–756 (1993).
5. B. Vernooij *et al.*, *Plant Cell* **6**, 959–965 (1994).
6. J. Malamy, D. F. Klessig, *Plant J.* **2**, 643–654 (1992).
7. R. F. White, *Virology* **99**, 410–412 (1979).
8. L. Friedrich *et al.*, *Plant J.* **10**, 61–70 (1996).
9. E. R. Ward *et al.*, *Plant Cell* **3**, 1085–1094 (1991).
10. Q. Li *et al.*, *Nat. Commun.* **14**, 6848 (2023).
11. S. W. Park, E. Kaimoyo, D. Kumar, S. Mosher, D. F. Klessig, *Science* **318**, 113–116 (2007).
12. H. W. Jung, T. J. Tschaplinski, L. Wang, J. Glazebrook, J. T. Greenberg, *Science* **324**, 89–91 (2009).
13. R. Chaturvedi *et al.*, *Plant J.* **71**, 161–172 (2012).
14. B. Chanda *et al.*, *Nat. Genet.* **43**, 421–427 (2011).
15. M. Hartmann *et al.*, *Cell* **173**, 456–469.e16 (2018).
16. Y. C. Chen *et al.*, *Proc. Natl. Acad. Sci. U.S.A.* **115**, E4920–E4929 (2018).
17. T. Sun *et al.*, *Nat. Commun.* **6**, 10159 (2015).
18. E. C. Holmes, Y. C. Chen, M. B. Mudgett, E. S. Sattely, *Plant Cell* **33**, 750–765 (2021).
19. L. Mohnike *et al.*, *Plant Cell* **33**, 735–749 (2021).
20. M. Hartmann, J. Zeier, *Curr. Opin. Plant Biol.* **50**, 44–57 (2019).
21. M. Löwe *et al.*, *Front. Plant Sci.* **14**, 1217771 (2023).
22. S. Bauer *et al.*, *Plant Cell* **33**, 714–734 (2021).
23. A. Kachroo, P. Kachroo, *Curr. Opin. Plant Biol.* **58**, 41–47 (2020).
24. H. Návarová, F. Bernsdorff, A. C. Döring, J. Zeier, *Plant Cell* **24**, 5123–5141 (2012).
25. X. Y. Zheng *et al.*, *Proc. Natl. Acad. Sci. U.S.A.* **112**, 9166–9173 (2015).

26. H. Li, J. Qiu, X. D. Fu, *Curr. Protoc. Mol. Biol.* **98**, 14.13.1–4.13.9 (2012).
27. Y. Zhang *et al*., *Proc. Natl. Acad. Sci. U.S.A.* **107**, 18220–18225 (2010).
28. J. L. Pruneda-Paz, G. Breton, A. Para, S. A. Kay, *Science* **323**, 1481–1485 (2009).
29. U. Dubiella *et al*., *Proc. Natl. Acad. Sci. U.S.A.* **110**, 8744–8749 (2013).
30. M. A. Torres, J. D. G. Jones, J. L. Dangl, *Nat. Genet.* **37**, 1130–1134 (2005).
31. M. A. Torres, J. L. Dangl, *Curr. Opin. Plant Biol.* **8**, 397–403 (2005).
32. D. Lee *et al*., *Nat. Commun.* **11**, 1838 (2020).
33. M. E. Alvarez *et al*., *Cell* **92**, 773–784 (1998).
34. R. W. King, J. A. Zeevaart, *Plant Physiol.* **53**, 96–103 (1974).
35. A. M. Maldonado, P. Doerner, R. A. Dixon, C. J. Lamb, R. K. Cameron, *Nature* **419**, 399–403 (2002).
36. P. Carella *et al*., *Plant Physiol.* **171**, 1495–1510 (2016).
37. S. Li, *Plant Signal. Behav.* **10**, e1044192 (2015).
38. I. L. Viola, L. N. Güttlein, D. H. Gonzalez, *Plant Physiol.* **162**, 1434–1447 (2013).
39. D. Rekhter *et al*., *Science* **365**, 498–502 (2019).
40. M. P. Torrens-Spence *et al*., *Mol. Plant* **12**, 1577–1586 (2019).
41. C. I. Murray, J. E. Van Eyk, *Circ. Cardiovasc. Genet.* **5**, 591 (2012).
42. S. Ahmad *et al*., *Front. Biosci. (Schol. Ed.)* **9**, 71–87 (2017).
43. E. Kuźniak, H. Urbanek, *Acta Physiol. Plant.* **22**, 195–203 (2000).
44. Y. Fichman, S. I. Zandalinas, S. Peck, S. Luan, R. Mittler, *Plant Cell* **34**, 4453–4471 (2022).
45. V. Houot *et al*., *J. Exp. Bot.* **52**, 1721–1730 (2001).
46. J. Chen *et al*., *Nature* **613**, 145–152 (2023).
47. C. F. Wei *et al*., *Plant J.* **51**, 32–46 (2007).
48. S. Akter *et al*., *Nat. Chem. Biol.* **14**, 995–1004 (2018).
49. Z. Chen, H. Silva, D. F. Klessig, *Science* **262**, 1883–1886 (1993).
50. U. Neuenschwander *et al*., *Plant J.* **8**, 227–233 (1995).
51. M. C. Wildermuth, J. Dewdney, G. Wu, F. M. Ausubel, *Nature* **414**, 562–565 (2001).
52. H. M. Yuan, W. C. Liu, Y. T. Lu, *Cell Host Microbe* **21**, 143–155 (2017).
53. Y. Fichman, G. Miller, R. Mittler, *Mol. Plant* **12**, 1203–1210 (2019).
54. S. I. Zandalinas *et al*., *Proc. Natl. Acad. Sci. U.S.A.* **117**, 13810–13820 (2020).
55. D. Laporte *et al*., *J. Exp. Bot.* **63**, 503–515 (2012).
56. M. Riedlmeier *et al*., *Plant Cell* **29**, 1440–1459 (2017).
57. J. Qi, J. Wang, Z. Gong, J. M. Zhou, *Curr. Opin. Plant Biol.* **38**, 92–100 (2017).
58. M. B. Shine *et al*., *Sci. Adv.* **8**, eabm8791 (2022).
59. C. Wang *et al*., *Sci. Adv.* **4**, eaar4509 (2018).
60. M. Delledonne, J. Zeier, A. Marocco, C. Lamb, *Proc. Natl. Acad. Sci. U.S.A.* **98**, 13454–13459 (2001).
61. C. Wang *et al*., *Cell Rep.* **7**, 348–355 (2014).
62. M. El-Shetehy *et al*., *Plant Signal. Behav.* **10**, e998544 (2015).
63. T. E. Mishina, J. Zeier, *Plant Physiol.* **141**, 1666–1675 (2006).
64. B. Jing *et al*., *Plant Physiol.* **157**, 973–980 (2011).
65. H. Yoo *et al*., *Mol. Plant* **13**, 88–98 (2020).
66. F. Bernsdorff *et al*., *Plant Cell* **28**, 102–129 (2016).
67. I. Yildiz *et al*., *Plant Physiol.* **186**, 1679–1705 (2021).
68. S. Karapetyan, M. Mwimba, X. Dong, bioRxiv 2023.04.21.535069 [Preprint] (2023); https://doi.org/10.1101/2023.04.21.535069
69. M. Mwimba *et al*., *Nat. Commun.* **9**, 4290 (2018).
70. W. Wang *et al*., *Nature* **470**, 110–114 (2011).
71. V. Bhardwaj, S. Meier, L. N. Petersen, R. A. Ingle, L. C. Roden, *PLOS ONE* **6**, e26968 (2011).

ACKNOWLEDGMENTS

We thank J. Pruneda-Paz for WT (*CCA1$_P$:LUC*), *che-1* (*CCA1$_P$:LUC*), *lhy-20* (*CCA1$_P$:LUC*), and *che-1 lhy-20* (*CCA1$_P$:LUC*) mutant lines. We thank P. Zhou, M. Li, and C. F. Schmidt for their help in measuring H_2O_2 levels. We also thank Z. Li at the Duke Proteomics and Metabolomics Core Facility for measuring SA, Pip, NHP, and G3P. **Funding:** This work was funded by National Institutes of Health grant NIH 1R35GM118036 (X.D.), National Science Foundation grants NSF IOS-1645589 and IOS-2041378 (X.D.), the Howard Hughes Medical Institute (HHMI) (X.D.), a Hargitt postdoctoral fellowship (L.C., H.Y.), and National Science Foundation MCB-2109302 (S.K.). **Author contributions:** Conceptualization: L.C., H.Y., X.D.; Methodology: L.C., T.C., S.K., S.K., X.D.; Investigation: L.C., H.Y., T.C., M.M., X.Z., S.K.; Funding acquisition: L.C., H.Y., S.K., X.D.; Supervision: X.D.; Writing – original draft: L.C., X.D.; Writing – review and editing: L.C., T.C., X.Z., S.K., H.Y., X.D. **Competing interests:** X.D. is a founder of Upstream Biotechnology, Inc., and a member of its scientific advisory board and is also a scientific advisory board member of Inari Agriculture, Inc., and Aferna Bio. **Data and materials availability:** All generated materials in the manuscript are available upon request. All data are available in the main text or the supplementary materials.

SUPPLEMENTARY MATERIALS

science.org/doi/10.1126/science.adj7249
Materials and Methods
Figs. S1 to S9
Tables S1 to S3
References (*72*–*81*)
MDAR Reproducibility Checklist
Movies S1 to S7

Submitted 12 July 2023; resubmitted 16 April 2024
Accepted 5 July 2024
10.1126/science.adj7249